Comparative study of cell mechanics methods

Dikla Raz-Ben Aroush[1], Atef Asnacios[2], Wei-Chiang Chen[3], Maxim E. Dokukin[4], Bryant L. Doss[5], Pauline Durand[2], Andrew Ekpenyong[6], Jochen Guck[6], NataliiaV. Guz[9], Paul A. Janmey[1], Nicole M. Moore[8], Albrecht Ott[7], Yeh-Chuin Poh[8], Robert Ros[5], Mathias Sander[7], Igor Sokolov[4], Jack R. Staunton[5], Ning Wang[8], Graeme Whyte[6], Denis Wirtz[3], Pei-Hsun Wu[3*]

[1]Institute for Medicine and Engineering, University of Pennsylvania, 1010 Vagelos Laboratories, 3340 Smith Walk, Philadelphia, Pennsylvania 19104, USA

[2]Laboratoire Matière et Systèmes Complexes, Unité Mixte de Recherche 7057, Centre National de la Recherche Scientifique (CNRS) and Université Paris-Diderot (Paris 7), Sorbonne Paris Cité, CC7056-10, Rue A. Domont et L. Duquet, 75205 Paris Cedex 13, France

[3]Department of Chemical and Biomolecular Engineering and Departments of Pathology and Oncology, The Johns Hopkins University and Johns Hopkins School of Medicine, Baltimore, Maryland, 21218, USA

[4]Department of Mechanical Engineering, Tufts University, Medford, Massachusetts 02155, USA

[5]Department of Physics, Arizona State University, Tempe, Arizona 85287, USA

[6] Biotechnology Center, Technische Universität Dresden, Dresden, Germany

[7]Saarland University, Biological Experimental Physics Department, P.O. Box 151150, 66041 Saarbruecken, Germany

[8]Department of Mechanical Science and Engineering, College of Engineering, University of Illinois at Urbana-Champaign, Urbana, Illinois 61801, USA

[9] Department of Physics, Clarkson University, Potsdam, New York 13699, USA

Abstract

Cell mechanics controls important cellular and subcellular functions, including cell adhesion, migration, polarization, and differentiation, as well as organelle organization, and trafficking inside the cytoplasm. Yet, reported values of cell stiffness and viscosity vary strongly, suggesting disagreements. To address this issue and illustrate the complementarity of different instruments, we present, analyze, and critically compare measurements conducted by some of the most widely used methods of cell mechanics: atomic force microscopy, magnetic twisting cytometry, particle-tracking microrheology, parallel-plates rheometry, cell monolayer rheology, and optical stretcher. These measurements highlight that elastic and viscous moduli of breast cancer cell MCF-7 can vary 1,000 fold and 100 fold, respectively. We discuss the sources of these variations, including the level of applied mechanical stress and rate of deformation, the geometry of the probe, the location probed in the cell, and the extracellular microenvironment.

Introduction

Cells *in vivo* are continuously subjected to mechanical forces, including **shear**, **compressive**, and **extensional forces** (words highlighted in bold are defined in glossary; Fig. 1). The ability of cells to deform and actively respond to physical forces is critical to proper embryonic development and the homeostasis of adult tissues and organs. Cell mechanics is the factor that defines cell response to the mechanical forces exercised by the cell microenvironment, including other cells and the extracellular matrix [1]. This cellular response can be **viscous**, **elastic**, or **viscoelastic**, as well as **passive** or **active**. Cell mechanics controls important cellular and subcellular functions, including cell adhesion, migration, polarization, and differentiation, as well as organelle organization, trafficking inside the cytoplasm, and activity. The recent translation of tools developed to measure cell mechanics has revealed that changes in cell and nuclear mechanics are hallmarks of many human diseases, particularly metastatic cancer, cardiovascular disease, inflammation, laminopathies, host-microbe interactions in infectious diseases, and frailty in aging [2-6]. Yet, values of cell elasticity (which measures the stretchiness of cells) and viscosity (which measures viscous dissipation) reported in the literature vary strongly even when different groups use the same instruments, suggesting disagreements. A contributor to these variations is often attributed to differences in cell culture conditions (e.g. sometimes subtle differences in temperature, pH, cell passage number, etc.), which prevent direct comparisons among datasets and may have slowed down the translation of cell-mechanics instruments for clinical applications.

To address these issues and illustrate the great complementarity of different instruments, we present, analyze, and critically compare measurements conducted by different research groups using different instruments, applied to the same commonly used MCF-7 human breast cancer cells cultured in the same environmental conditions *in vitro*. The instruments tested include some of the most widely used methods of cell mechanics: atomic force microscopy (AFM), magnetic twisting cytometry (MTC), particle-tracking microrheology (PTM), parallel-plates rheometry, cell monolayer rheology (CMR), and optical stretching (OS).

Overall, though the underlying mechanical principles remain the same, our measurements highlight how cell mechanics depends exquisitely on the level of mechanical **stress** and rate of deformation to which the cell is subjected, the geometry of the mechanical probe used in the experiments, the probe-cell contact area, the probed location in the cell (e.g. cell cortex, nucleus, lamella, cytoplasm), and the cellular context (e.g. monolayer of cells *vs*. single cells, adherent *vs*. free-floating cells, etc.). These results also highlight how mechanical properties of cells can vary by orders of magnitude depending on the length scale at which cell **viscoelasticity** is probed, from tens of nanometers (e.g. the size of an actin fiber) to several microns (the size of a whole cell). In addition, we review the advantages and the time required for each instrument, the type of cells and length and time scales that can be probed.

Results

To ensure consistency, the measurements presented below were conducted in different laboratories on MCF-7 cells from the same lot, cultured in medium from the same lot, all directly provided by ATCC. The mechanical properties of these cells were measured by a total of eight laboratories using AFM, MTC, PTM, parallel-plates rheometry, CMR and OS. Details of the techniques used by the participating laboratories can be found in Table S1. Different moduli were measured from different methods and detailed description of moduli and their inter-relationship can be found in **supplemental information**. Among the methods tested in this study, AFM, parallel plates, and OS can all provide direct measurements of the Young's modulus (E), while MTC, CMR and PTM all provide measurements of the shear modulus (G).

AFM

AFM-based indentation is a commonly used technique to quantify the mechanical properties of adherent cells with subcellular resolution. An AFM consists of a cantilever of calibrated stiffness applying a preset force or deformation at a defined speed onto an adherent cell or tissue and, through laser deflection and detection by a photodetector (Fig. 2a), measures the corresponding resisting force from the deformation of the cell (Fig. 2b). A 3D piezo scanner allows for x, y, and z displacements of the cantilever relative to the underlying cell (Fig. 2a). Here, MCF7 cells are indented by either nanoscale pyramidal probes (radius of the probe apex ~10 nm), mesoscale spheroconical probes (~750 nm) or microscale spherical probes (~ 5 μm) (Fig. 2c).

The **elastic** (*effective* **Young's**) **modulus** of the cells is quantified by fitting the curves of the measured force as a function of the vertical position of the cantilever using so-called elastic contact models that account for the geometry of indentation (see supplementary information). When measured with a nanoscale AFM probe, the mechanical properties of cells are highly heterogeneous and display large cell-to-cell variations (Fig. 2, d and e). For indentations of ~1 μm produced at a speed of 2 μm/s with a sharp tip – which are both typical – the average static effective Young elastic modulus of MCF-7 cells over the central nuclear region was 5.5 ± 0.8 kPa (kiloPascal) and 3.8 ± 0.5 kPa over flat regions of the cell body, between the nucleus and the cell edge. Measurements at a higher indentation speed resulted in higher elastic moduli of 10.5 ± 0.5 kPa (Fig. 2, c-e).

By indenting cells with a larger probe (Fig. 2f), AFM measurements are less sensitive to local cell heterogeneities and the elastic modulus is significantly lower. Probes with an intermediate apex radius (~0.75 μm) which transitions to an axisymmetric cone to indent the nuclear region applied at a speed of 2 μm/s yielded an elastic modulus of 0.58 ± 0.23 kPa when computed using the "blunted indenter" contact model [7,8]. Applying the Hertz model of indentation[9], 5-μm diameter glass beads attached to tipless cantilevers (Fig.2, h,i) and indentation depth of ~ 300 nm yielded elastic moduli of 0.53 ± 0.52 kPa for an indentation speed of 10 μm/s at 37° C and 0.81 ± 0.06 kPa for 6 μm/s at room temperature.

Whole-cell deformation measurements

Once MCF7 cells are detached from their underlying substrates, they round up (similarly to cancer cells in blood vessels after intravasation) and can be kept alive in suspension for a few hours. To measure the viscoelastic properties of cells in suspension, methods that preserve this suspended state are required, including the parallel-plates rheometer and the OS:

Parallel-plates rheometer. The parallel-plates rheometer extracts the Young (**extensional) modulus** and deformability (i.e. **compliance**) at the global cellular scale [10]. A single cell is placed between a rigid plate and a flexible plate of calibrated stiffness k used as a force probe and stretched via computer control through constant or oscillatory displacements (Fig. 3a). For oscillatory displacements of the plates of frequency ω (Fig. 1), the elastic (storage) and viscous (loss) moduli, $E'(\omega)$ and $E''(\omega)$, were observed to be weak power laws of the frequency, $E'(\omega) \sim E''(\omega) \sim \omega^{\alpha}$ with $\alpha << 1$ (Fig. 3b). The exponent α of this power law estimates the balance between dissipative and elastic behaviors: A higher exponent signifies higher viscous dissipation; in particular, $\alpha = 0$ for a purely elastic solid (e.g. rubber), while $\alpha = 1$ for a viscous liquid (e.g. water). The **viscous modulus** of MCF-7 cells at a frequency of 1Hz was $E_0'' = 340 \pm 40$ Pa, the **elastic modulus** was $E_0' = 950 \pm 150$ Pa (Fig. 3, c and d), and $\alpha = 0.18 \pm 0.01$, indicating a predominantly elastic response.

The parallel-plates rheometer also measures the **relaxation** and **creep** functions of individual cells, i.e. the stress evolution under constant strain and the deformation under constant stress, respectively. MCF-7 cells showed a weak power-law behavior with an extensional modulus $E_0 = \sqrt{E_0'^2 + E_0''^2} = 1020 \pm 150$ Pa at 1 Hz (Fig. S1). Moreover, when applying static cell elongations and measuring the corresponding lateral cell deformations, we found a **Poisson's ratio** $\nu = 0.33$. The shear modulus could be estimated to be $G_0 = E_0/2(1+\nu) = 380$ Pa at 1 Hz.

Optical stretcher (OS). The OS consists of a dual-beam optical trap capable of inducing well-defined mechanical **stresses** on whole cells in suspension, to measure the creep compliance and modulus of single cells [2 11,12]. The forces that trap and deform the cell outwardly (Fig. 3e) arise from the change in the refractive index, RI, at the cell-medium interface and the ensuing transfer of momentum from the light to the cell [12]. The average RI = 1.374 ± 0.002 of MCF7 cells was measured by digital holographic microscopy [13] (Fig. S2d). The stress on the cells is computed using an electromagnetic wave model [14]. For convenient delivery of the cells into the trapping region, the OS is integrated in a microfluidic system (Fig. 3e), which enables measurement rates > 100 cells/h.

In this study, MCF7 cells were analyzed after each cell was trapped for 2 s at a power of 0.2 W per fiber and stretched for 8 s at 0.75 W per fiber. We obtained an average peak **strain** (at $t = 8$ s) of 5.16 ± 0.11% (Fig. 3f.) and the average peak compliance (i.e. deformability) was 0.053 ± 0.001 Pa^{-1} (Fig. 3f). The creep compliance profile reveals the composite viscous and elastic properties of cells. The white triangle (Fig. 3f) indicated a clear linear increase of strain (i.e. deformation) with time, demonstrating a dominant viscous behavior when cells are in suspension. The inverse of the slope enables a first estimation of steady-state viscosity, which we found to be about 180 Pa.s. Fitting using finer models [2] yields a viscosity of 158 ± 84 Pa.s (Fig. 3g). We note here that this overwhelming dominance of viscosity over elasticity is not a feature of all cell types as measured in the OS. Even with MCF7 cells, stretching at higher laser powers produced creep curves with more pronounced elastic components (see Fig.S2d).

Multicellular measurements

Cell monolayer rheology (CMR) consists of cells placed between two plates of a commercial rotational rheometer with a glass sensor of plate-ring geometry [15]. Fibronectin coating (2 μg/cm^2) of the plates enhances cell adhesion; cells form a sparse monolayer observed through a

microscope during measurements (Fig. 4a). The ring rotates around its symmetry axis, which leads to the simultaneous **shear deformation** of the cells by about the same amount. At an oscillation frequency of 0.5 Hz, MCF7 cells exhibit a decrease in **shear modulus** with increasing amplitude of the imposed shear deformation. The cell shear modulus G at a relative deformation of 0.1 is G = 4.6 ± 2.2 kPa. Assuming a Poisson ratio of 0.3, the cell elastic (stretching) modulus was E = 12 ± 5.7 kPa. We extracted elastic and viscous contributions to the cell shear modulus from the phase shift between excitation and cell response, G' = 4.5 ± 2.2 kPa and G'' = 1.1 ± 0.5 kPa, corresponding to elastic and viscous stretching moduli Y' = 12 ± 5.7 kPa and Y'' = 3.9 ± 2.9 kPa (Fig. 4). At a constant relative deformation of 0.02, the cell shear modulus increased with increasing oscillation frequency to fit a power law with an exponent β=0.065. Under constant load, single-cell creep compliances followed a power law in time with an exponent that decreased with increasing stress from approximately 0.1 to 0.01 (see **supplementary information**).

Bead-based measurements

The magnetic twisting cytometer (MTC). The MTC utilizes an RGD-coated ferromagnetic magnetic bead bound to the apical surface of the MCF-7 cell (Fig 5a) [12], [13]. A controlled homogeneous magnetic field is then applied around the cell via magnetic coils, causing the bead to displace and rotate. Based on the magnitude of the bead-cell area of contact (Fig 5b), magnetic field applied (Fig 5c), and the displacement of the magnetic bead (Fig 5c), the MCF-7 cell stiffness is quantified [14, 15]. The shear modulus of MCF-7 cells was $G_0 = \sqrt{G_0'^2 + G_0''^2}$ = 0.69 ± 0.05 kPa; the elastic modulus was G' = 0.62 ± 0.04 kPa and the viscous modulus was G'' = 0.25 ± 0.02 kPa. Assuming a Poison's ratio of 0.3, the Young modulus of MCF-7 cells was E_0=1.78 ± 0.12 kPa, the elastic modulus was E'=1.62 ± 0.11 kPa, and the viscous modulus was E''= 0.66 ± 0.06 kPa (Fig 5d).

Particle-tracking microrheology (PTM). In PTM, sub-micron fluorescent beads are ballistically injected into the cytoplasm or nucleus; the cells are then allowed to recover in fresh medium overnight [16]. The spontaneous movements of the beads inside the cells are recorded with ~5 nm spatial resolution, typically at video rate for 20 s [16-18]. The mean square displacements (MSDs) of beads were computed from the bead trajectories (Fig 5e-g). The ensemble-averaged MSDs from three different cell-culture plates were identical (Fig 5h). Student t-test showed that there was no significant difference in elastic modulus from three different plates measured at 30 Hz, suggesting consistent and reproducible results (Fig 5i). At 1 Hz, the elastic modulus was G' = 4.5 ± 0.4 Pa and the viscous modulus was G'' = 10.1 ± 0.9 Pa. The creep compliance is proportional to the MSD of a bead embedded in the cell (Fig 5k). Therefore, the creep compliance of the cytoplasm of MCF-7 could also be calculated from the MSDs of the beads (Fig 5l).

Discussion

Mechanical forces are increasingly recognized as major regulators of cell phenotypes and tissue and organ formation and organization. The modulus of a cell - its viscoelastic properties - is a key factor in how cells sense these forces and interact with other cells and the extracellular matrix. In this study, the mechanical properties of a cell are here measured by different methods, including AFM, PTM, OS, CMR, MTC, and parallel-plates rheometry. In principle, different types of rheological measurements should be related to each other if certain assumptions about the materials being measured are valid, yet the average values of moduli vary by at least two orders of magnitude (Table 1). In general, the results presented in table 1 can be divided in three categories by the values of the obtained modulus: small (OS, PTM), intermediate (AFM with dull probes, parallel-plates rheometry, MTC), and high (AFM with a sharp probe, CMR). This range demonstrates the complex mechanical behavior of cells in response to forces and highlights the importance of choosing the correct technique depending on the biological question being addressed (Table S1). These methods differ widely in how the measurements are collected and what area of the cell is probed (Table S1) which in part could explains this huge differences. Below, we discuss the reasons for similarities and variations among different measurements.

#Limitation of results (system error).
#model assumption not valid (cell as prooelastic but model often assume linear elastaic and/or viscoelastic; continuity)
#Measuring parameters affecting measurement outcome
cytophysiological state of cell when measurement 1) suspension vs adhesion, 2) activate mechanical signaling
#pre-stress (tip shape of AFM)
Cell transient response to the measurement

Assumption from Model inferred results

The viscoelastic moduli of cells are generally not direct measurement from different methods but inferred from physical models in which certain assumption are introduced, such as linear elasticity for AFM or viscoelastic behavior for the other methods. For cells, these assumptions are at best only partially satisfied – e.g., the cell cortex, cytoplasm and nucleus each have uniquely different characteristics. Consequently, errors may be introduced in transforming the primary data into the material properties. For AFM, discrepancies can arise from the choice of models that typically range within other sources of systematic error (e.g. cantilever calibration errors ~10-15%). One common assumption imposed in the model is that the cell is treated as a homogeneous, isotropic, linear, viscoelastic material [1]. The second assumption underlying most mechanical measurements of cells is that the Poisson's ratio is close to 0.5, or at least is a constant. Recent work indicates that the cytoplasm of living cells can behave as a poroelastic material, which could potentially result in errors in estimating moduli from primary data[32]. For each method, there are more specific assumptions is imposed. Taking MTC as an example, one typically assumes values for the surface area of the bead in direct contact with the cell.

Cytophysiological state of cell at probing

The elasticity of MCF-7 cells measured by OS was more than two orders of magnitude smaller than the elasticity measured by AFM, MTC, and parallel-plates rheometer. The major difference between OS and the other techniques is in the cell adhesion: OS works with free-floating cells, whereas the other methods use cells adhered to a rigid glass substrate. Although it is expected that cells change their cytoskeleton, and presumably their mechanical properties, after adhesion, it was shown that weakly adherent MCF-7 cells do not significantly change their modulus [27]. This implies that complete detachment of cells from the surface substantially "relaxes" cells.

MTC and the CMR employ an "active" mechanical measurement where specific ligands are used. MTC utilizes beads that are coated with RGD peptides, while CMR has fibronectin-coated plates to engage specific transmembrane integrins in cell adhesion. In such conditions, the cellular cytoskeleton is connected to integrins cell-receptors through focal adhesion complexes, and tensile forces are generated in the cell structure and transmitted to its substrate (in particular to the mechanical probe). Although not done in this study, parallel-plates rheometry and AFM are capable of active mechanical measurements on mechanically active (i.e. tensed) cells by functionalizing the surfaces with specific ligands, and high tensile forces were indeed measured in these conditions[10,35,36].

Pre-stress

Pre-stressed conditions can increase the apparent elastic modulus of cells, the modulus increasing roughly linearly with the pre-stress [37]. Mechanical measurements can then propagate deeply into the cell through prestress and stiff actin bundles that guide the propagation of forces over long distances [34]. In CMR, the measured elastic modulus is about an order of magnitude higher than the ones obtained from other contact probe based methods. This can presumably be explained by the existence of a tensile pre-stress in CMR in which cells are probably applying high tensile forces in between the plates [10,35,36]. One order of magnitude increase in the apparent elastic modulus, as measured with MCR, is consistent with the typical tensile stresses measured on single cells. It is also consistent with the observations of substantially higher modulus in AFM experiments when using the sharp conical AFM probe. Such probe produces much higher stresses compared to the use of the dull probes. As a result, the cell material presumably becomes overstretched and becomes stiffer. This is similar to what was observed on other soft materials and viscoelastic polymer solutions [38].

Measuring parameters

The response of a living cell to a mechanical stimulus depends on how it is applied. Oscillating CMR yields a notable decrease of the cell modulus with increasing amplitude regardless whether it is deformation (also called strain) or stress that is controlled. Moduli measured by AFM show a rather large difference when measured with sharp or dull AFM probes (Fig.2). These can be explained by substantial difference in the stresses imposed by such probes onto the cell. In addition, AFM allows measuring the moduli's dependence on the indentation depth though there is no clear overall trend, and both increasing and decreasing moduli occur. Cells are known to exhibit stiffening as well as softening and the complex interplay between the two is still far from understood.

Besides the size of the probe, cells are also sensitive to the probed timescales. Passive and active microbead rheology show that cell moduli increase with frequency. This is in good

agreement with the parallel-plates rheometer as well as CMR results. They yield moduli that increase with frequency as a weak power-law with an exponent in the range of 0.01-0.25. Cell deformability (also called compliance) obtained from creep experiments also increases as a weak power law with time. The exponents are similar to those obtained from frequency sweeps as measured by the parallel-plates rheometer and CMR. The CMR study shows that the exponent depends on the applied stress (see supplementary information). The OS also yields a power-law increase for cell compliance. However, the exponent is 0.85, close to one, indicating a mostly viscous behavior of the cells. This is presumably because the OS probes cells in suspension, for which the main force-bearing structures of the attached cell – stress fibers and focal adhesions – are absent.

A deformation of controlled amplitude and frequency defines a rate. We observe that the cell response is highly dependent on the rate of deformation. For AFM measurements, indentation speeds can be varied between 2 and 10 μm/s. However, no clear dependence of the moduli on the rate can be inferred. This may be attributed to the fact that the modulus was measured at a relatively large indentation of 1μm. This means that the pericellular layer of cell was squeezed and, consequently, we probed the mechanics of the cell body. As was recently found for neuronal cells[26], the mechanics of the cell body is independent of the indentation speed for indentation rates of 1–10 μm/s, which is similar to the range used in this paper. Cell monolayer rheology probes cell responses to shear stress ramp cycles of different speeds. A pronounced hysteresis between loading and unloading occurs for slow rates of stress increase or decrease. The amplitude of the hysteresis corresponds to the amount of energy that is absorbed by the cell in a loading and unloading cycle. Hysteresis vanishes above a threshold rate and the cell deformation is almost dissipation-free. We suggest that above a certain stress rate cytoskeletal bonds do not reform [33], and the cell exhibits a mostly elastic response. Cellular moduli may vary by up to an order of magnitude depending on size, frequency, and rate of the mechanical cues, which can be probed with the different experimental approaches described in this work.

Using MTC as an example, primary data include the known torque applied to each bead, and its resulting displacement. For this case, one typically assumes values for the surface area of the bead in direct contact with the cell (or the contact area can be measured by staining the ligand or the receptor or the nearby recruited proteins), that the cell can be treated as a homogeneous, isotropic, linear, viscoelastic material [15], and that the stresses generated by the twisting torque is directly transmitted to the cell regardless of the receptor/ligand interactions used to attach the bead. Most of the same assumptions apply to the interpretation of data from AFM measurements, where the primary data are generally uniaxial force and displacement, and calculations of material constants account for the complex strain field due to the tip geometry.

A number of analytical and approximate models are used for pyramidal, conical, spherical, blunted, and spheroconical tips, wherein the power law exponent varies from ½ (conical) to 3/2 (spherical). Discrepancies arising from the choice of model typically range within other sources of systematic error (e.g. cantilever calibration errors ~10-15%) and from the assumption that shear and Young's moduli are simply related (see glossary), since AFM probes typically result in spatially complex strains fields that combine shear, compression, and stretch [23,24]. These models yield an elastic modulus, which assume a homogeneous, isotropic, and linear elastic material. In the quasistatic deformations used here, (indentation rates ~1 – 10 μm/s) cells

characteristically exhibit an elastic response at which viscous dissipation is minute. Dynamic mechanical analysis whereby the AFM tip is oscillated over a range of frequencies while in contact with cell can also be conducted, yielding a complex (i.e. viscous and elastic) modulus [29,30]. In cases where specific adhesion is strong, contact area is increased, changing the strain field, for which other models may be used [31]. If these assumptions are valid, the computed elastic modulus values are precise and accurate; but for cells, these assumptions are at best only partially satisfied – e.g., the cell cortex, cytoplasm and nucleus each have uniquely different characteristics. Consequently, errors may be introduced in transforming the primary data into the material properties. Similar assumptions are made in the calculation of moduli from other experimental methods [22]. Further, recent work indicates that the cytoplasm of living cells can behave as a poroelastic material, which could potentially result in errors in estimating moduli from primary data[32].

Comparison between different methods

The measurements using the large AFM probes are physically quite similar to the whole-cell measurements using parallel-plates rheometry. The values of the elastic modulus derived by large AFM probes and parallel-plates are similar (see table 1) possible due to physically they are quite similar While forces are applied to the cell directly due to physical contact in AFM, the parallel plates apply forces through molecular links developed between the plates and the cell body.

The measurements were conducted by different research groups, which could potentially lead to differences in measured viscoelastic moduli due, for instance, to variations in processing cell samples even though the source of cell were tightly controlled. However, the average values of moduli vary by at least two orders of magnitude (Table 1), a variation that is unlikely to result from variations in sample processing (cell culture, medium, etc.). This range demonstrates the complex mechanical behavior of cells in response to forces and highlights the importance of choosing the correct technique depending on the biological question being addressed (Table S1). These methods have complementary advantages and disadvantages (Table S1).

The cell is a highly heterogeneous object. While it is plausible to characterize the cell with just an average “effective” elastic modulus, AFM and PTM can probe different regions of the cell, creating maps of mechanical properties of cells. The cell nucleus is typically harder than the cell periphery [19]. Moreover, the cell is surrounded by a pericellular coat, a layer of glycocalyx and membrane protrusions. When a probe approaches the cells, it deforms the pericelluar coat and cell body at the same time. Using a special “brush model” [19,20], one can derive the parameters of the pericelluar coat, such as the brush size and density, by analyzing the AFM force data. Furthermore, the mechanical properties of cells embedded in 3D-tissue environments can be quantified by advanced data analysis techniques [8,21].

Comparison between different methods

In principle, different types of rheological measurements should be related to each other if certain assumptions about the materials being measured are valid. It is likely that some discrepancies in the literature arise from assuming that cells and other biological materials are

linear elastic continuous solids. Cells, however, are far from being isotropic, and real measurements require finite, sometimes large strains to obtain reliable force data. Nearly all measurements by surface indentation, for instance, assume the validity of the equation relating *E* and *G* because the deformation in such measurements is a complex combination of uniaxial and shear deformations that change with indentation depth and probe geometry. Recent measurements on macroscopic biological samples suggest that Young's and shear moduli are not simply related under the conditions of many studies. For example, Young's and shear moduli during macroscopic measurements of biopolymer networks such as collagen networks [22,23] and intact biological tissues [24,25] become uncoupled from each other at deformations as small as a few percent. Since the typical deformations applied by AFM probes and possibly also magnetic tweezers are far larger than this value, these measurements are likely to depend on the extent to which uniaxial and shear deformations dominate the deformation, a quantity that is usually unknown.

The measurements using the large AFM probes are physically quite similar to the whole-cell measurements using parallel-plates rheometry. The values of the elastic modulus derived by both methods are indeed not substantially different (see table 1). Smaller values derived from the AFM measurements can be explained by examining the difference in the physics of the probe-cell contact in these two methods. While forces are applied to the cell directly due to physical contact in AFM, the parallel plates apply forces through molecular links developed between the plates and the cell body. Physical indentation of the cell with the AFM probe implies squeezing of both the pericellular coat and the cell body itself. Since the pericellular coat is effectively softer than the cell body [26,27], the AFM values of the elastic modulus are expected to be smaller than the values obtained by parallel-plates rheometry. Using a more complicated model, which takes into account the presence of the pericellular layer [20], it is possible to derive the elastic modulus of the cell body in the AFM experiments. As one can see from ref [28], the values obtained within such a model for MFC-7 cells (0.95±0.26 kPa) are virtually identical to the values obtained with the parallel-plates rheometer (0.95 ± 0.15 kPa, see Table 1).

AFM can also be directly compared with MTC. Similar to the parallel-plates approach, the contact between the magnetic bead and cell is due to molecular linkages between the bead and pericellular membrane. However, the modulus derived from MTC data is about ~60% higher than even the one derived from parallel-plates rheometer. This could be explained by the fact that the effective area of the contact between the magnetic bead and cell is higher than assumed due to additional contact between the beads and microscopic roughness of the pericellular membrane (microvilli and microridges).

The second assumption underlying most mechanical measurements of cells is that the Poisson's ratio is close to 0.5, or at least is a constant. However as is well-documented in the literature for tissues such as cartilage, many biological materials are highly poroelastic, with stresses relaxing as fluid flows out of a compressed network or into a stretched network, allowing the polymers to adopt lower energy states. In macroscopic rheological measurements of elasticity, poroelasticity is often negligible because the fluid permeation is so slow that the volume cannot change during the measurements on a time scale of a second or so. However, measurements of cells by nanoscale indenters deform very small volumes of material, and since the poroelastic relaxation time is a function of sample size, the rate in which fluid flows out of the deformed volume can be significant. In this case the assumption that the Poisson's ratio is a constant during the measurement is invalid and is likely to affect measurements that occur on different length scales or timescales.

Primary *vs*. model-based data

In an attempt to further compare our various measurement methods, physical models are used, and with these, certain assumptions are introduced, such as linear elasticity for AFM or viscoelastic behavior for the other methods. In this context, a distinction should be made between primary and unprocessed data, and the inference from these measurements on the parameters commonly used to describe the material properties of the cell.

Using MTC as an example, primary data include the known torque applied to each bead, and its resulting displacement. For this case, one typically assumes values for the surface area of the bead in direct contact with the cell (or the contact area can be measured by staining the ligand or the receptor or the nearby recruited proteins), that the cell can be treated as a homogeneous, isotropic, linear, viscoelastic material [15], and that the stresses generated by the twisting torque is directly transmitted to the cell regardless of the receptor/ligand interactions used to attach the bead. Most of the same assumptions apply to the interpretation of data from AFM measurements, where the primary data are generally uniaxial force and displacement, and calculations of material constants account for the complex strain field due to the tip geometry.

A number of analytical and approximate models are used for pyramidal, conical, spherical, blunted, and spheroconical tips, wherein the power law exponent varies from ½ (conical) to 3/2 (spherical). Discrepancies arising from the choice of model typically range within other sources of systematic error (e.g. cantilever calibration errors ~10-15%) and from the assumption that shear and Young's moduli are simply related (see glossary), since AFM probes typically result in spatially complex strains fields that combine shear, compression, and stretch [23,24]. These models yield an elastic modulus, which assume a homogeneous, isotropic, and linear elastic material. In the quasistatic deformations used here, (indentation rates ~1 – 10 μm/s) cells characteristically exhibit an elastic response at which viscous dissipation is minute. Dynamic mechanical analysis whereby the AFM tip is oscillated over a range of frequencies while in contact with cell can also be conducted, yielding a complex (i.e. viscous and elastic) modulus [29,30]. In cases where specific adhesion is strong, contact area is increased, changing the strain field, for which other models may be used [31]. If these assumptions are valid, the computed elastic modulus values are precise and accurate; but for cells, these assumptions are at best only partially satisfied – e.g., the cell cortex, cytoplasm and nucleus each have uniquely different characteristics. Consequently, errors may be introduced in transforming the primary data into the material properties. Similar assumptions are made in the calculation of moduli from other experimental methods [22]. Further, recent work indicates that the cytoplasm of living cells can behave as a poroelastic material, which could potentially result in errors in estimating moduli from primary data[32].

Effects of mechanical stress and frequency (measurement parameter effect)

The response of a living cell to a mechanical stimulus depends on how it is applied. Oscillating CMR yields a notable decrease of the cell modulus with increasing amplitude regardless whether it is deformation (also called strain) or stress that is controlled. Moduli measured by AFM show a rather large difference when measured with sharp or dull AFM probes (Fig.2). These can be explained by substantial difference in the stresses imposed by such probes onto the cell. In addition, AFM allows measuring the moduli's dependence on the indentation depth though there is no clear overall trend, and both increasing and decreasing moduli occur. Cells are known to

exhibit stiffening as well as softening and the complex interplay between the two is still far from understood.

Besides the size of the probe, cells are also sensitive to the probed timescales. Passive and active microbead rheology show that cell moduli increase with frequency. This is in good agreement with the parallel-plates rheometer as well as CMR results. They yield moduli that increase with frequency as a weak power-law with an exponent in the range of 0.01-0.25. Cell deformability (also called compliance) obtained from creep experiments also increases as a weak power law with time. The exponents are similar to those obtained from frequency sweeps as measured by the parallel-plates rheometer and CMR. The CMR study shows that the exponent depends on the applied stress (see supplementary information). The OS also yields a power-law increase for cell compliance. However, the exponent is 0.85, close to one, indicating a mostly viscous behavior of the cells. This is presumably because the OS probes cells in suspension, for which the main force-bearing structures of the attached cell – stress fibers and focal adhesions – are absent.

A deformation of controlled amplitude and frequency defines a rate. We observe that the cell response is highly dependent on the rate of deformation. For AFM measurements, indentation speeds can be varied between 2 and 10 μm/s. However, no clear dependence of the moduli on the rate can be inferred. This may be attributed to the fact that the modulus was measured at a relatively large indentation of 1μm. This means that the pericellular layer of cell was squeezed and, consequently, we probed the mechanics of the cell body. As was recently found for neuronal cells[26], the mechanics of the cell body is independent of the indentation speed for indentation rates of 1–10 μm/s, which is similar to the range used in this paper. Cell monolayer rheology probes cell responses to shear stress ramp cycles of different speeds. A pronounced hysteresis between loading and unloading occurs for slow rates of stress increase or decrease. The amplitude of the hysteresis corresponds to the amount of energy that is absorbed by the cell in a loading and unloading cycle. Hysteresis vanishes above a threshold rate and the cell deformation is almost dissipation-free. We suggest that above a certain stress rate cytoskeletal bonds do not reform [33], and the cell exhibits a mostly elastic response. Cellular moduli may vary by up to an order of magnitude depending on size, frequency, and rate of the mechanical cues, which can be probed with the different experimental approaches described in this work.

Adherent *vs.* free-floating cells

The elasticity of MCF-7 cells measured by OS was more than two orders of magnitude smaller than the elasticity measured by AFM, MTC, and parallel-plates rheometer. The major difference between OS and the other techniques is in the cell adhesion: OS deals with free-floating cells, whereas the other methods use cells adhered to a rigid glass substrate. Although it is expected that cells change their cytoskeleton, and presumably their mechanical properties, after adhesion, it was shown that weakly adherent MCF-7 cells do not significantly change their modulus [27]. This implies that complete detachment of cells from the surface substantially "relaxes" cells. It should b~~e noted that the OS is the ideal technique to assess the mechanical properties of naturally suspended cells, such as blood cells or circulating tumor cells.~~ The cells being in suspension also enables higher measurement throughput (> 100 cells/h) compared to techniques where cells are attached to a substratum.

Dependency of mechano-transduction signaling

Pre-stressed conditions can increase the apparent elastic modulus of cells, the modulus increasing roughly linearly with the pre-stress [37].

MTC and the CMR employ an "active" mechanical measurement where specific ligands are used. MTC utilizes beads that are coated with RGD peptides, while CMR has fibronectin-coated plates to engage specific transmembrane integrins in cell adhesion. In such conditions, the cellular cytoskeleton is connected to integrins cell-receptors through focal adhesion complexes, and tensile forces are generated in the cell structure and transmitted to its substrate (in particular to the mechanical probe). Mechanical measurements can then propagate deeply into the cell through prestress and stiff actin bundles that guide the propagation of forces over long distances [34]. Parallel-plates rheometry, PTM, AFM, and OS probe relaxed cells since no extracellular matrix proteins are engaged. However, although not done in this study, parallel-plates rheometry and AFM are capable of active mechanical measurements on mechanically active (i.e. tensed) cells by functionalizing the surfaces with specific ligands, and high tensile forces were indeed measured in these conditions[10,35,36]. In CMR, the measured elastic modulus is about an order of magnitude higher than the ones obtained from other contact probe based methods. This can presumably be explained by the existence of a tensile pre-stress in CMR. Indeed, since the plates of the rheometer are coated with fibronectin and cells left to spread before measurement, cells are probably applying high tensile forces in between the plates [10,35,36]. Such a pre-stress is known to increase the apparent elastic modulus of cells, the modulus increasing roughly linearly with the pre-stress [37]. In this context, one order of magnitude increase in the apparent elastic modulus, as measured with MCR, is consistent wiffth the typical tensile stresses measured on single cells. It is also consistent with the observations of substantially higher modulus in AFM experiments when using the sharp conical AFM probe. Such probe produces much higher stresses compared to the use of the dull probes. As a result, the cell material presumably becomes overstretched and becomes stiffer. This is similar to what was observed on other soft materials and viscoelastic polymer solutions [38].

Dependence of cell mechanics and cellular processes on time scales

The cytoskeleton is a dynamic biopolymer network whose material properties are different when probed at short and long timescales [39,4041]. Overall duration that each cell is subjected to probing can affected measurement results from time-scale dependent cellular processes. Frequency and probing durations for different method are summarized in supplemental Table X. The probing duration can range from 4s with OS to 2 hours in CMR.

The results would be expected to be different owing to changes taking place in each cell during the time of probing.

Signaling, transcription processes and protein synthesis (which alter cell state and architecture) can take different amount of time to process (minutes for phosphorylation and hours for transcription) . Actin polymerization and cytoskeletal remodeling also take place in seconds [42]. Changes in cell mechanics and cell shape to effect protrusion and migration takes place in minutes [43]. Taking a closer look at the timescales involved in various cellular processes, one would find it justifiable to think of 'time factor' in cell functions involving mechanical properties.

The 'time factor' may well turn out to be one of the sources of some of the similarities and differences in the results. It becomes necessary to care about the duration of mechanical perturbation to which each the cell is subjected during measurement, in view of the time evolution of the property involved [44], as a clear example of time-dependent changes in cell deformability. At the same time, the change of mechanical properties is not necessarily large. AFM measurements of human epithelial skin cells showed virtually the same modulus during continuous measurements for about 2.5 h [45].

Limitation of the results

Though the goal of this work is to directly compare different cell mechanical methods by probing the same type of cells with minimal biological variations, systematic errors may arise from the different instrumentations setups, which could also contribute to the observed wide spectrum of results. For example, distinct from other methods presented here, sample heating is one of primary source of systematic error for OS. Cells measured with OS at different temperatures (e.g. induced by the stretching laser) leads to a shortening of the time-scales at which the cells respond. The impact for the measurement here is that the OS as used in the present study (laser wavelength 1064 nm) likely led to heating, which has in turn led to a more viscous response of the cells. It should be noted that this is not due to biological change (via transcription or signaling, for example as a heat-shock response of cells), but a purely material response during the short duration of the measurement. The temperature is back to ambient temperature as soon as the laser is turned off [46]. The potential source of systematic error has beene discussed in the literature, for PTM in [47,48], for AFM in [38], for MTC in [49,50], and for parallel plates in [51]. Importantly, the reported systematic relative error is in general < 20%, while the observed difference in measured elastic moduli from these different methods can be as high as 3,000 fold.

Furthermore, in the present study, we found that AFM and PTM contribute to the highest and lowest elastic moduli measured among the six tested methods. The results were in the same range as shown in a previous study in which mechanical properties of non-tumorigenic breast epithelial MCF-10A and tumorigenic breast cancer cell MDA-MB-231 were assessed by AFM and PTM [52]. The Youngs' modulus of MDA-MB-231 and MCF10A cells measured by AFM was ~ 0.2-1.6 kpa, depending on the cell type and probe location. Resulting MSD profiles from PTM were also in the similar scale as the one measured in the current comparative study. Therefore, the measurement spread between different cell mechanical assays is less likely to be due to method-dependent systematic errors, and more likely to be due to the level of mechanical **stress** and rate of deformation to which the cell is subjected, the geometry of the mechanical probe used in the experiments, the probe-cell contact area, the probed location in the cell (e.g. cell cortex, nucleus, cytoplasm), and the cellular context (e.g. monolayer of cells *vs*. single cells, adherent *vs*. free-floating cells, etc.).

Choice of methods for different biological contexts

The proper choice of a cell-mechanics method depends critically on the biological context and the biological process of interest (Table S1). All tested methods can probe cell samples *in vitro* and *ex vivo.* However, only MTC and PTM can be directly extended to probing mechanics of cells in tissues *in vivo* or fully embedded in 3D extracellular matrices since, for both methods, the probes (i.e. the probe particles) are remotely monitored through optics and no direct contact is required from cell mechanics.

Unlike other methods, OS measures cells in suspension, without physical contact with a probe, but OS cannot probe the micromechanics of cells adherent on 2D substrates or embedded in 3D tissues and matrices. OS is an ideal choice for measuring blood-borne cells at single-cell resolution. All six methods can provide single-cell resolution, but measurement throughput can vary from <10 (parallel plates, AFM) to ~2,000 (MTC) cells per hour (Table S1). For cell samples with known large variations, higher throughput measurements, such as MTC and OS (~100 cells per hour), may overcome sample variations by collecting large datasets.

One other important factor to consider is the mechanical context associated with the biological question being asked. If the differences being investigated are local or are rapid changes in the cytosol, using PTM may provide the more sensitive readout. To probe changes in cortical tension (for instance following cell spreading), MTC is particularly well suited (Table S1).

Other mechanical measurement methods

The current study does not cover the whole spectrum of cellular mechanic measurement methods. Several new techniques have recently been developed to measure cell mechanical properties at high speed. Particularly, the incorporation of microfluidic-based methods and use of confined channels provide convenient ways to exercise forces and deform cells [53-56] and reach extremely high throughput rates, ranging between 10 – 10,000 cells/sec. This opens an entirely new and practical dimension to cell mechanics research. However, most of these techniques do not provide a direct measurement of Young's modulus which makes inter-comparison between techniques difficult. In addition, there are new optics-based non-invasive methods for measuring mechanical properties, such as Brillouin microscopy that can extract mechanical information about cells and tissues at sub-micrometer resolution [57,58]. This method also does not provide a direct measurement of the Young's modulus.

~~**Future directions**~~

~~Although an attempt has been made here to incorporate measurements in a variety of conditions, most still are performed on cells adherent to a flat, rigid surface. One important exception to this is the measurement by optical stretching, in which the cell is suspended in solution during measurement. Moreover, PTM can measure cell mechanics within a three-dimensional tissue, surrounded by a compliant extracellular matrix. However, studies have reported important differences associated with a 3D microenvironment, ranging from differences in the cytoskeletal structure and in the nature of intracellular signaling associated with migration [59,60].~~

~~In all measurement methods discussed here, the cell has been perturbed to some extent to make the measurement – beads are introduced, or cells are pushed or prodded in various ways, which can have important consequences on cell function through mechanotransduction [61]. Methods need to be developed that are entirely non-intrusive, that probe the cell with minimal (or no) effects on biological function. One example would be by monitoring the random, thermally-induced motions of internal cell structures (e.g., mitochondria), similar to what is done with ballistic injection nanorheology, but with particles intrinsic to the cell.~~

Acknowledgments

This research was supported by grants from the NIH CA210173 (DW and PHW), GM072744 (NW), GM096971 (PJ), CA193417 (PJ), CA143862 (RR), the NSF #1510700 (RR), and funding from Agence Nationale de la Recherche ("ImmunoMeca" ANR-12-BSV5-0007-01) (AA), "Initiatives d'excellence" Idex ANR-11-IDEX-0005-02 (AA), "Labex Who Am I?" ANR-11-LABX-0071 (AA), the Deutsche Forschungsgemeinschaft through the collaborative research center SFB1027 (AO).

References

1 Lautenschlager, F. *et al.* The regulatory role of cell mechanics for migration of differentiating myeloid cells. *Proceedings of the National Academy of Sciences of the United States of America* **106**, 15696-15701, doi:10.1073/pnas.0811261106 (2009).

2 Guck, J. *et al.* Optical deformability as an inherent cell marker for testing malignant transformation and metastatic competence. *Biophys J* **88**, 3689-3698 (2005).

3 Wirtz, D., Konstantopoulos, K. & Searson, P. C. The physics of cancer: the role of physical interactions and mechanical forces in metastasis. *Nature reviews. Cancer* **11**, 512-522, doi:10.1038/nrc3080 (2011).

4 Lammerding, J. *et al.* Lamin A/C deficiency causes defective nuclear mechanics and mechanotransduction. *The Journal of clinical investigation* **113**, 370-378, doi:10.1172/JCI19670 (2004).

5 Phillip, J. M., Aifuwa, I., Walston, J. & Wirtz, D. The Mechanobiology of Aging. *Annu Rev Biomed Eng* **17**, 113-141, doi:10.1146/annurev-bioeng-071114-040829 (2015).

6 Bufi, N. *et al.* Human Primary Immune Cells Exhibit Distinct Mechanical Properties that Are Modified by Inflammation. *Biophysical Journal* **108**, 2181-2190, doi:10.1016/j.bpj.2015.03.047 (2015).

7 Briscoe, B. J., Sebastian, K. S. & Adams, M. J. The effect of indenter geometry on the elastic response to indentation *J Phys D Appl Phys* **27**, 1156-1162 (1994).

8 Staunton, J. R., Doss, B. L., Lindsay, S. & Ros, R. Correlating confocal microscopy and atomic force indentation reveals metastatic cancer cells stiffen during invasion into collagen I matrices. *Sci Rep-Uk* **6** (2016).

9 Hertz, H. Über den Kontakt elastischer Körper. *Zeitschrift fur Orthopadie und Unfallchirurgie* **92**, 156-171, doi:10.1055/s-0034-1382860 (1882).

10 Thoumine, O. & Ott, A. Time scale dependent viscoelastic and contractile regimes in fibroblasts probed by microplate manipulation. *Journal of cell science* **110 (Pt 17)**, 2109-2116 (1997).

11 Guck, J. *et al.* The optical stretcher: a novel laser tool to micromanipulate cells. *Biophys J* **81**, 767-784, doi:10.1016/S0006-3495(01)75740-2 (2001).

12 Guck, J., Ananthakrishnan, R., Moon, T. J., Cunningham, C. C. & Kas, J. Optical deformability of soft biological dielectrics. *Physical review letters* **84**, 5451-5454 (2000).

13 Chalut, K. J., Ekpenyong, A. E., Clegg, W. L., Melhuish, I. C. & Guck, J. Quantifying cellular differentiation by physical phenotype using digital holographic microscopy. *Integrative biology : quantitative biosciences from nano to macro* **4**, 280-284, doi:10.1039/c2ib00129b (2012).

14 Boyde, L., Chalut, K. J. & Guck, J. Interaction of Gaussian beam with near-spherical particle: an analytic-numerical approach for assessing scattering and stresses. *Journal of the Optical Society of America. A, Optics, image science, and vision* **26**, 1814-1826 (2009).

15 Fernandez, P., Heymann, L., Ott, A., Aksel, N. & Pullarkat, P. A. Shear rheology of a cell monolayer. *New J Phys* **9** (2007).

16 Wirtz, D. Particle-tracking microrheology of living cells: principles and applications. *Annual review of biophysics* **38**, 301-326, doi:10.1146/annurev.biophys.050708.133724 (2009).

17 Wu, P. H. *et al.* High-throughput ballistic injection nanorheology to measure cell mechanics. *Nature protocols* **7**, 155-170, doi:10.1038/nprot.2011.436 (2012).

18 Lee, J. S. *et al.* Ballistic intracellular nanorheology reveals ROCK-hard cytoplasmic stiffening response to fluid flow. *Journal of cell science* **119**, 1760-1768, doi:10.1242/jcs.02899 (2006).
19 Sokolov, I., Iyer, S., Subba-Rao, V., Gaikwad, R. M. & Woodworth, C. D. Detection of surface brush on biological cells in vitro with atomic force microscopy. *Applied Physics Letters* **91**, 023902-023901-023903 (2007).
20 Sokolov, I., Dokukin, M. E. & Guz, N. V. Method for quantitative measurements of the elastic modulus of biological cells in AFM indentation experiments. *Methods* **60**, 202-213, doi:DOI 10.1016/j.ymeth.2013.03.037 (2013).
21 Zhou, X. M. *et al.* Fibronectin fibrillogenesis regulates three-dimensional neovessel formation. *Gene Dev* **22**, 1231-1243, doi:10.1101/gad.1643308 (2008).
22 Vahabi, M. *et al.* Elasticity of fibrous networks under uniaxial prestress. *Soft matter* **12**, 5050-5060, doi:10.1039/c6sm00606j (2016).
23 van Oosten, A. S. *et al.* Uncoupling shear and uniaxial elastic moduli of semiflexible biopolymer networks: compression-softening and stretch-stiffening. *Sci Rep-Uk* **6**, 19270, doi:10.1038/srep19270 (2016).
24 Perepelyuk, M. *et al.* Normal and Fibrotic Rat Livers Demonstrate Shear Strain Softening and Compression Stiffening: A Model for Soft Tissue Mechanics. *PloS one* **11**, e0146588, doi:10.1371/journal.pone.0146588 (2016).
25 Pogoda, K. *et al.* Compression stiffening of brain and its effect on mechanosensing by glioma cells. *New J Phys* **16**, 075002, doi:10.1088/1367-2630/16/7/075002 (2014).
26 Simon, M. *et al.* Load Rate and Temperature Dependent Mechanical Properties of the Cortical Neuron and Its Pericellular Layer Measured by Atomic Force Microscopy. *Langmuir* **32**, 1111-1119, doi:10.1021/acs.langmuir.5b04317 (2016).
27 Guz, N., Dokukin, M., Kalaparthi, V. & Sokolov, I. If cell mechanics can be described by elastic modulus: study of different models and probes used in indentation experiments. *Biophys J* **107**, 564-575, doi:10.1016/j.bpj.2014.06.033 (2014).
28 Dokukin, M. E., Guz, N. V. & Sokolov, I. Quantitative Study of the Elastic Modulus of Loosely Attached Cells in AFM Indentation Experiments. *Biophys J* **104**, 2123-2131, doi:10.1016/j.bpj.2013.04.019 (2013).
29 Mahaffy, R. E., Shih, C. K., MacKintosh, F. C. & Kas, J. Scanning probe-based frequency-dependent microrheology of polymer gels and biological cells. *Physical review letters* **85**, 880-883 (2000).
30 Alcaraz, J. *et al.* Microrheology of human lung epithelial cells measured by atomic force microscopy. *Biophysical Journal* **84**, 2071-2079 (2003).
31 Johnson, K. L., Kendall, K. & Roberts, A. D. Surface Energy and Contact of Elastic Solids. *Proc R Soc Lon Ser-A* **324**, 301-&, doi:DOI 10.1098/rspa.1971.0141 (1971).
32 Moeendarbary, E. *et al.* The cytoplasm of living cells behaves as a poroelastic material. *Nat Mater* **12**, 253-261, doi:10.1038/NMAT3517 (2013).
33 Xu, J. Y., Tseng, Y. & Wirtz, D. Strain hardening of actin filament networks - Regulation by the dynamic cross-linking protein alpha-actinin. *J Biol Chem* **275**, 35886-35892, doi:DOI 10.1074/jbc.M002377200 (2000).
34 Poh, Y. C. *et al.* Generation of organized germ layers from a single mouse embryonic stem cell. *Nature communications* **5**, 4000, doi:10.1038/ncomms5000 (2014).
35 Mitrossilis, D. *et al.* Single-cell response to stiffness exhibits muscle-like behavior. *Proceedings of the National Academy of Sciences of the United States of America* **106**, 18243-18248, doi:10.1073/pnas.0903994106 (2009).

36 Mitrossilis, D. *et al.* Real-time single-cell response to stiffness. *Proceedings of the National Academy of Sciences of the United States of America* **107**, 16518-16523, doi:10.1073/pnas.1007940107 (2010).
37 Kollmannsberger, P. & Fabry, B. High-force magnetic tweezers with force feedback for biological applications. *The Review of scientific instruments* **78**, 114301, doi:10.1063/1.2804771 (2007).
38 Dokukin, M. E. & Sokolov, I. On the Measurements of Rigidity Modulus of Soft Materials in Nanoindentation Experiments at Small Depth. *Macromolecules* **45**, 4277-4288, doi:Doi 10.1021/Ma202600b (2012).
39 Deng, L. *et al.* Fast and slow dynamics of the cytoskeleton. *Nature materials* **5**, 636-640, doi:10.1038/nmat1685 (2006).
40 Xu, J., Tseng, Y. & Wirtz, D. Strain hardening of actin filament networks. Regulation by the dynamic cross-linking protein alpha-actinin. *J Biol Chem* **275**, 35886-35892, doi:10.1074/jbc.M002377200 (2000).
41 Ekpenyong, A. E. *et al.* Viscoelastic properties of differentiating blood cells are fate- and function-dependent. *PloS one* **7**, e45237, doi:10.1371/journal.pone.0045237 (2012).
42 Yap, B. & Kamm, R. D. Cytoskeletal remodeling and cellular activation during deformation of neutrophils into narrow channels. *Journal of applied physiology* **99**, 2323-2330, doi:10.1152/japplphysiol.00503.2005 (2005).
43 Stroka, K. M., Hayenga, H. N. & Aranda-Espinoza, H. Human neutrophil cytoskeletal dynamics and contractility actively contribute to trans-endothelial migration. *PloS one* **8**, e61377, doi:10.1371/journal.pone.0061377 (2013).
44 Frank, R. S. Time-dependent alterations in the deformability of human neutrophils in response to chemotactic activation. *Blood* **76**, 2606-2612 (1990).
45 Berdyyeva, T. K., Woodworth, C. D. & Sokolov, I. Human epithelial cells increase their rigidity with ageing in vitro: direct measurements. *Physics in medicine and biology* **50**, 81-92 (2005).
46 Ebert, S., Travis, K., Lincoln, B. & Guck, J. Fluorescence ratio thermometry in a microfluidic dual-beam laser trap. *Opt Express* **15**, 15493-15499, doi:Doi 10.1364/Oe.15.015493 (2007).
47 Savin, T. & Doyle, P. S. Static and dynamic errors in particle tracking microrheology. *Biophysical Journal* **88**, 623-638, doi:10.1529/biophysj.104.042457 (2005).
48 Wu, P. H., Arce, S. H., Burney, P. R. & Tseng, Y. A Novel Approach to High Accuracy of Video-Based Microrheology. *Biophysical Journal* **96**, 5103-5111, doi:10.1016/j.bpj.2009.03.029 (2009).
49 Gosse, C. & Croquette, V. Magnetic tweezers: Micromanipulation and force measurement at the molecular level. *Biophysical Journal* **82**, 3314-3329 (2002).
50 Wong, W. P. & Halvorsen, K. The effect of integration time on fluctuation measurements: calibrating an optical trap in the presence of motion blur. *Opt Express* **14**, 12517-12531, doi:Doi 10.1364/Oe.14.012517 (2006).
51 Desprat, N., Richert, A., Simeon, J. & Asnacios, A. Creep function of a single living cell. *Biophysical Journal* **88**, 2224-2233, doi:10.1529/biophysj.104.050278 (2005).
52 Agus, D. B. *et al.* A physical sciences network characterization of non-tumorigenic and metastatic cells. *Scientific Reports* **3**, doi:Artn 1449
10.1038/Srep01449 (2013).
53 Gossett, D. R. *et al.* Hydrodynamic stretching of single cells for large population mechanical phenotyping. *Proceedings of the National Academy of Sciences of the United States of America* **109**, 7630-7635, doi:10.1073/pnas.1200107109 (2012).

54 Byun, S. *et al.* Characterizing deformability and surface friction of cancer cells. *Proceedings of the National Academy of Sciences of the United States of America* **110**, 7580-7585, doi:10.1073/pnas.1218806110 (2013).
55 Lange, J. R. *et al.* Microconstriction Arrays for High-Throughput Quantitative Measurements of Cell Mechanical Properties. *Biophysical Journal* **109**, 26-34, doi:10.1016/j.bpj.2015.05.029 (2015).
56 Mietke, A. *et al.* Extracting Cell Stiffness from Real-Time Deformability Cytometry: Theory and Experiment. *Biophysical Journal* **109**, 2023-2036, doi:10.1016/j.bpj.2015.09.006 (2015).
57 Scarcelli, G. *et al.* Noncontact three-dimensional mapping of intracellular hydromechanical properties by Brillouin microscopy. *Nat Methods* **12**, 1132-+, doi:10.1038/nmeth.3616 (2015).
58 Elsayad, K. *et al.* Mapping the subcellular mechanical properties of live cells in tissues with fluorescence emission-Brillouin imaging. *Sci Signal* **9**, doi:ARTN rs5
10.1126/scisignal.aaf6326 (2016).
59 Fraley, S. I., Feng, Y., Giri, A., Longmore, G. D. & Wirtz, D. Dimensional and temporal controls of three-dimensional cell migration by zyxin and binding partners. *Nature communications* **3**, 719, doi:10.1038/ncomms1711 (2012).
60 Fraley, S. I. *et al.* A distinctive role for focal adhesion proteins in three-dimensional cell motility. *Nature cell biology* **12**, 598-604, doi:10.1038/ncb2062 (2010).
61 Wang, N., Butler, J. P. & Ingber, D. E. Mechanotransduction across the cell surface and through the cytoskeleton. *Science* **260**, 1124-1127 (1993).

Figure captions

Figure 1: Description on rheological tests. (a) Different geometries of deformation. To test the mechanical properties of a material, one can either stretch/compress it (left), or apply a shear mechanical stress (right). While stretching, deformation of the material results from applying a pulling force F perpendicular to the surface of the sample. For a surface of area A, the applied (normal) stress is given by $\sigma = F/A$, and the deformation (or strain) in the direction of the applied force is $\varepsilon = \Delta L/L_o$, and $\Delta L = L\text{-}L_0$ is the sample elongation along the direction of stretching. Similarly, compression corresponds to a deformation (shortening) that results from applying a pushing force perpendicular to the surface area. In contrast, a shear test implies deformations that occur when the applied force is parallel (tangential) to the surface of the sample. **(b)** Constant or oscillating applied stress: A creep test consists in applying a constant stress F_0/A overtime and recording the resulting deformation $\varepsilon(t)$ of the sample (left). For a dynamic test, the applied force oscillates resulting in an oscillatory deformation of the sample (right). Creep allows one to directly access the response of the sample at different time scales, but may lead to high deformations that may permanently transform the material. Thus, oscillations are generally used to investigate the behavior of the sample at small deformations. The measurements are carried out at different frequencies ("frequency sweep") to analyze the response of the sample at different time scales. **(c)** Viscoelasticity: The mechanical response of any material can be described in terms of two ideal behaviors, those of an elastic solid and a viscous liquid. Purely elastic solids, like springs, deform instantaneously and in proportion to the applied force. In creep, the strain sets instantaneously to its equilibrium value ε_f. In dynamic tests, the deformation follows the oscillating applied stress, meaning that there is no phase shift between $\varepsilon(t)$ and $\sigma(t)$ signals. In both tests, the ratio between stress and strain is constant and corresponds to the elastic modulus $E = \sigma/\varepsilon$, which is expressed in Pascals (Pa), like a pressure. E quantifies the rigidity of the material. Like springs, solids with high E are harder to deform. Purely viscous fluids, like water, will flow indefinitely when subjected to a creep test. The rate $d\varepsilon/dt$ at which the liquid flows under a given stress σ_0 depends on its viscosity η, $\delta\varepsilon/\delta\tau = \sigma_o/\eta$. For instance, honey displays a higher viscosity than water and is thus harder to flow. In dynamic tests, the oscillating deformation is delayed compared to the applied oscillating stress, and the phase shift between $\varepsilon(t)$ and $\sigma(t)$ signals is $\Delta t = T/4$, where T is the period of the oscillations. The amplitudes of stress and strain are then related by $\sigma = (2\pi f\eta)\varepsilon$, where $f = 1/T$ is the frequency of the oscillations. Thus $(2\pi f\eta)$ has the dimension of a modulus, and quantifies the viscous response depending on the frequency of the test (example of water skiing, with water becoming hard like ice when deformed at high speed!) Most materials are viscoelastic and share characteristics of both elastic solids and viscous liquids. Depending on the time scale (or, equivalently, on the frequency), the elastic or viscous-like behavior may dominate the response of such a material. For instance, when submitted to a creep test, the particular sample represented on the figure will flow like a liquid at short times, but its deformation will reach, at long times, an equilibrium value characteristic of elastic solids. In dynamic tests, the phase shift between $\varepsilon(t)$ and $\sigma(t)$ will be between 0 and $T/4$. The response of the viscoelastic sample is then quantified through a complex modulus $E^* = E' + i\,E''$, allowing one to decouple the elastic-like contribution E' (in-phase component of the response) from the viscous-like component E" (phase shift $\Delta t = T/4$). In the particular example of the figure, $E' = E$ the elastic modulus of springs, and $E'' = 2\pi f\eta$, where η is the viscosity of the surrounding liquid and f the frequency of the oscillations. Thus, at high

frequency (short times) $E'' > E'$ and the viscous behavior dominates, while at low frequency (long times) $E' > E''$ and the behavior is dominantly elastic, as observed from a creep test.

Figure 2. AFM measurements. The measurements were conducted using sharp conical AFM probes, conospherical probes of radius 750nm, and spherical probes of radius 2500nm. **(a)** Schematics of the measurements of the cell mechanics. An AFM probe of well-defined geometry indents a cell along the vertical z axis. **(b)** Shape of the force curves collected with AFM. Force *F vs*. vertical position *z* of the cell. Typical force curves for a mechanically soft and hard samples are shown. **(c)** Average elastic moduli obtained with various AFM probes under different conditions (vertical indenting speed *v* and surrounding temperature *T*) are shown. The error bar indicates one standard deviation. **(d, f, h)** Raw AFM force data (*F* versus *z*) obtained with the sharp conical probes (d), the dull conospherical probe (semi-vertical angle ~22.5°) (f), and the spherical probes (h). **(e, g, i)** Corresponding histograms and cumulative probabilities of the elastic modulus obtained for indentation depths of 0-300nm. The appropriate models were used for each type of the AFM probes: the Sneddon model for the sharp conical probes (e), the Hertz model for the dull conospherical probe (g), and the spherical probes (i). Sample temperatures and indenting speeds are shown in the histograms. AFM measurements and measured cell sample size are summarized in Table S2.

Figure 3. Whole-cell deformation measurements. (a-d): **cells between surfaces. (a**) Schematic of the parallel-plates rheometer. An oscillating displacement $D(\omega)$ is applied at the basis of the flexible microplate and the resulting displacement $d(\omega)$ at the tip of this microplate is recorded. The force applied to the cell is proportional to the flexible plate deflection δ: $F = k\delta$. The picture represents a side view of an MCF7 cell between the microplates. Scale bar, 10 μm. **(b)** Elastic (E', blue squares) and viscous (E'', red circles) extensional moduli as a function of frequency for a single MCF-7 cell in a log-log graph showing weak power-law behavior. **(c and d)** Distributions of viscous (c) and elastic (d) moduli (n = 18 cells). The mean values for viscous and elastic moduli were 340 ± 50 Pa and 950 ± 140 Pa, respectively. **(e)** Schematic of the OS: two diverging, counter-propagating laser beams emanating from single-mode optical fibers trap cells at low powers as they are being flowed into the trapping region using a microfluidic channel (left) and stretch them at higher powers (right). **(f).** Strain and compliance profiles for each cell measured in the OS. Cells (n = 514 cells) were trapped for 2 s at 0.2 W per fiber and stretched for 8 s (red portion of graph) at 0.75 W per fiber. The black curve shows average strain and compliance for the entire population. The average peak strain (at t = 8 s) was 5.16 ± 0.11%; the average peak compliance was 0.053 ± 0.001 Pa^{-1}. The white triangle indicates a linear increase of strain, suggesting a dominant viscous behavior. **(g)** Distribution of steady-state viscosity obtained by fitting the compliance results for each cell to the so-called standard linear liquid model. The average steady-state viscosity was 158 ± 84 Pa.s. **(h)** Distribution of elastic moduli obtained from the standard linear liquid model fitting, where the average elastic modulus obtained was 18 ± 24 Pa. Dotted lines represent cumulative distributions.

Figure 4: Cell monolayer rheology. (a) Schematic of the experimental setup. **(b)** Deformation-controlled amplitude sweep: the Young's modulus exhibits a decrease in cell stiffness with increasing oscillation amplitude at a constant frequency of 0.5 Hz. **(c)** Frequency sweep: cell shear modulus increases with increasing frequency at a constant shear deformation of 0.02 as a power law with exponent β=0.065. Inset: Cell elastic shear modulus G' and viscous modulus G"

at a frequency of 0.46 Hz is G' = 6.96 ± 2.3 kPa and G'' = 1.51 ± 0.89 kPa. Assuming a Poisson ratio of 0.3 we obtain elastic and viscous Young's moduli Y'=18 ± 6 kPa and Y''=3.9 ± 2.3 kPa (n = 8). Error bar represents standard deviation. (**d**) Creep experiments at different applied stress (insert). The creep compliances follow power laws. Exponents decrease with increasing stress from ~0.1 to 0.01 (data not shown). **(e).** Deformation-stress curves obtained from cyclic stress ramp experiments. We apply different rates of stress increase (insert). For low rates the deformation-stress curves exhibit nonlinear hysteresis (left x-axis, upper curve), which vanishes at high rates (right x-axis, lower curve).

Figure 5. Bead based measurements. (a-d) Magnetic twisting cytometry (MTC). (a) Schematic of the MTC. Dashed line denotes the position of the bead before twisting; white arrow indicates the direction of the bead magnetic moment. **(b**) Quantification of magnetic bead embedment in MCF7 cells. The bead embedment (~30%) was estimated by measuring the actin ring diameter from the fluorescent image and comparing it to the bead diameter from the brightfield image (double arrows). Scale bar, 10 μm**. (c)** Continuous magnetic field of 50 Gauss with a stress modulation (17.5 Pa peak stress) and displacements of the magnetic beads as a function of cyclic forces (0.3 Hz). For visual clarity, only data from 10 representative beads out of a total of 193 beads are shown. **(d)** Average elasticity of MCF-7 cell measured using MTC. Mean +/- SEM. **(e-m) Particle tracking microrheology (PTM). (e)** Representative MCF-7 phase contrast image with fluorescent beads after recovery. Scale bar, 15 μm. **(f).** Zoom-in image of a fluorescent bead (diameter, 100 nm) inside a cell. **(g)** Trajectory corresponding to the bead shown in panel f. Scale bar, 200 nm. **(h)** PTM is reproducible: 20 cells (>100 beads) were measured from each plate. **(i)** Ensemble-averaged MSDs from three different cell-culture plates were identical. **(j)** Two-sided Student t-test was applied on elastic modulus at 30 Hz measured from three different plates and showed there was no significant difference (p > 0.05). **(k)** Average elastic modulus of MCF-7 cells. Error bars indicate SEM. **(l)** Creep compliance of MCF-7 cells calculated from the bead MSDs. **m.** Distribution of MSDs (bars) and its cumulative distribution (dotted line).

Glossary

See also Fig. 1.

Stress – force per unit area; $\sigma = F / A$ SI unit is N/m^2

Strain –unitless parameter quantifying the extent of deformation after application of stress.

Compliance **(*J*)** – the relative extent to which a body yields to deflection by force, usually given by time dependent strain divided by constant stress

Shear Stress **(σ)** – force parallel to a material's axis per unit area; $\sigma = F / A$

Shear Strain **(γ)** –unitless parameter quantifying the extent of deformation after application of shear stress. For a cube, shear strain is ratio of lateral displacement over sample height. For other shapes, the form factor relates measured displacement to unitless strain.

Elongational Strain **(ε)** – fractional change in length or elongation; $\varepsilon = \delta / L$

Elasticity – the property of a material to deform to a defined extent in response to a force and then return to its original state when the force is removed

Viscosity **(η)** – measure of resistance of a fluid to deformation in response to shear stress; $\eta = \sigma / d\gamma/dt$

Young's modulus **(E)** – a constant describing a material's resistance to deformation in extension; $E = \sigma / \varepsilon$

Shear Modulus **(G)** – a constant describing a material's resistance to deformation in shear; $G = \sigma / \gamma$

Linear elasticity – Young's or shear modulus constant over range of strains, equivalently stress is proportional to strain.

Newtonian viscosity – viscosity independent of shear strain rate; linear relationship between shear stress and shear strain rate

Nonlinear elasticity – Young's or shear modulus that changes with strain

Non-Newtonian viscosity – viscosity dependent on shear strain rate; non-linear relationship between stress and strain rate (i.e. shear thickening or thinning)

Yield stress **(σ_y)** – maximum stress applicable to a system before rupture occurs

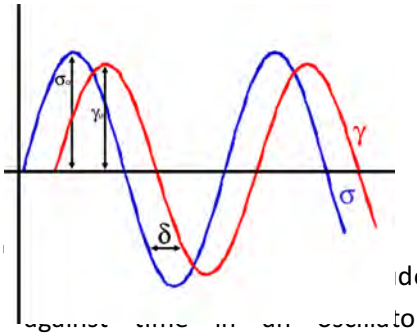

...des ...tory deformation. The stress and strain signals are phase shifted by an angle δ.

Poisson ratio (ν) – the ratio of transverse to axial strain when a material is deformed in stretch or compression. A material that conserves volume under strain has a Poisson ratio of 0.5. Materials with Poisson ratio less than 0.5 lose volume when compressed and gain volume when stretched. For linear elastic materials at small strain, Poisson's ratio relates shear and Young's moduli by the expression $E = 2G(1+\nu)$.

Dynamic viscoelasticity – Many time-dependent rheological measurements are made by applying a sinusoidally varying stress or a sinusoidally varying strain to a sample and measuring its strain or stress response, respectively, as a function of frequency. For linear materials, the result is two sinusoidal functions, and both the elastic and dissipative properties of the material are computed from the amplitudes and phase shifts of the sinusoidal functions.

Phase angle (δ) **–** The angular shift between the sinusoidally varying stress and strain in an oscillatory measurement. The value of δ is zero for a purely elastic solid and 90 degrees for a purely viscous liquid.

Elastic or storage modulus **(*G'*)** – measure of energy stored during a strain cycle; under sinusoidal conditions, the part of shear stress in phase with shear strain divided by shear strain; often expressed as the real part of the complex modulus: $G' = (\sigma_o / \gamma_o)*\cos(\delta)$

***Viscous of loss modulus* (*G*")** – measure of energy lost during a strain cycle; often expressed as the imaginary part of the complex modulus: $G'' = (\sigma_o / \gamma_o)*\sin(\delta)$

Table 1. Overview of measurements

Technique	**Results** *Elastic/storage modulus (kPa)* [*]	**Location of the measurement**	**Throughput**
AFM (tip size, temperature, loading rate)			
conical probe, 25 °C, 6 μm/s	13.5 ± 7.0	At the cell surface	1- 20 cells/h
conical probe, 37 °C, 2 μm/s	5.5 ± 0.8		
750 nm, 37 °C, 2 μm/s	0.58 ± 0.23		
2500 nm, 25 °C, 6 μm/s	1.31 ± 0.54		
2500 nm, 37 °C, 10 μm/s	0.53 ± 0.52		
Whole-cell measurements			
Optical stretcher	0.018 ± 0.024	Whole suspended cell	60 - 300 cells/h
Parallel plates (1 Hz)	0.95 ± 0.15	Whole adherent cell	6 cells/h
Cell monolayer measurements			
Cell monolayer rheology	6.9 ± 2.3	Monolayer of cells	5-6 h/monolayer
Bead-based measurements			
Particle tracking microrheology (1 Hz)	0.0045 ± 0.0004	Intracellular	30 cells/h
Particle tracking microrheology (30 Hz)	0.111 ± .002		
Magnetic twisting cytometry	1.62 ± 0.11	At the cell surface	2000 cells/h

[*] Elastic moduli derived from AFM represent effective Young's modulus.

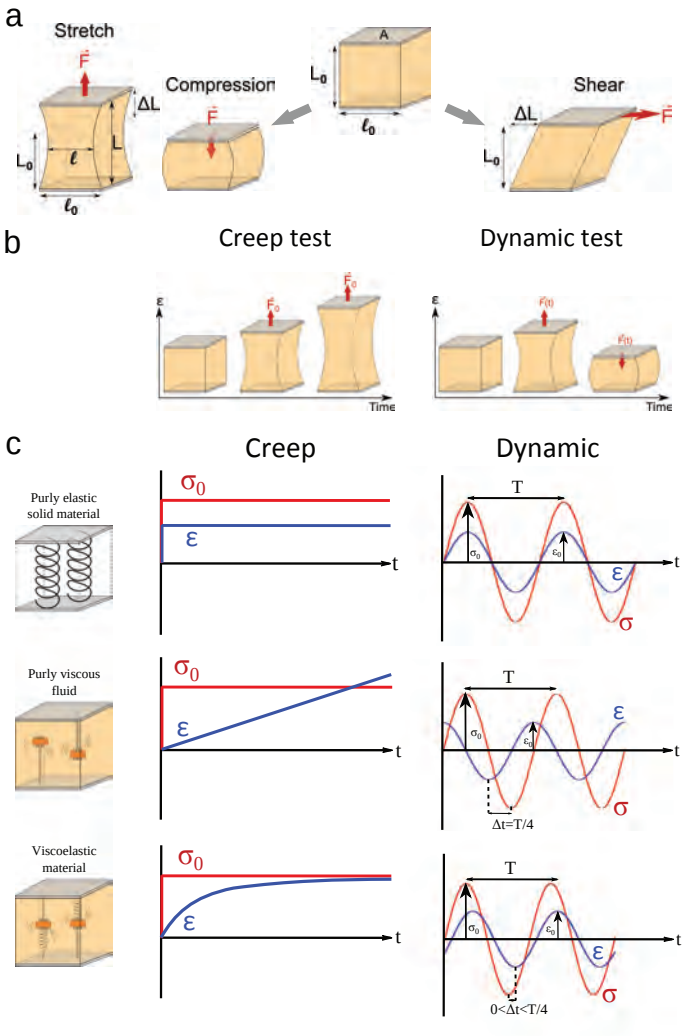
a
Stretch
Compression
Shear
ΔL
L
b
Creep test
Dynamic test
Time
c
Creep
Dynamic
Purly elastic solid material
Purly viscous fluid
Viscoelastic material
σ0
ε
t
T
Δt=T/4
0<Δt<T/4

Figure 1

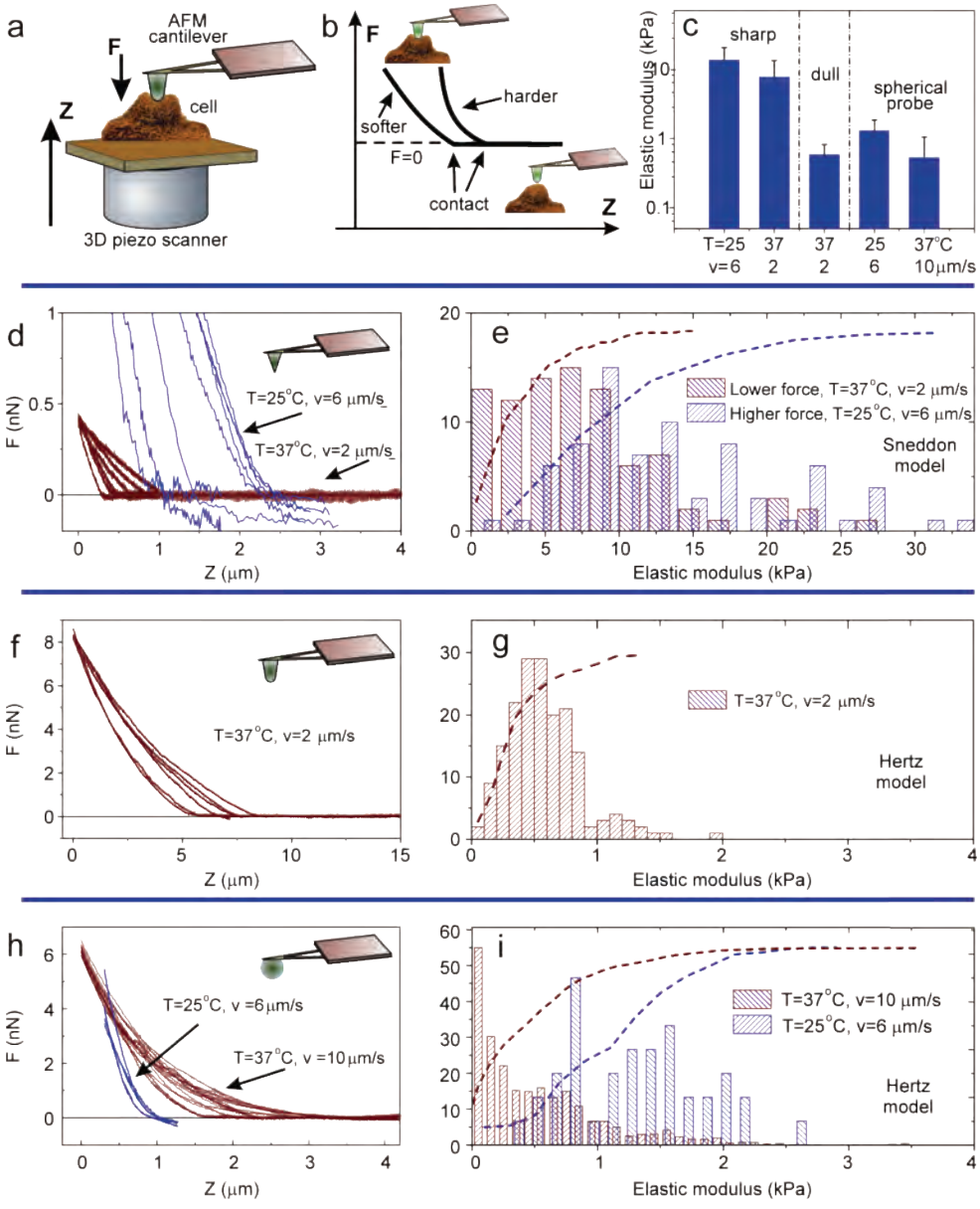
a
AFM cantilever
F
cell
z
3D piezo scanner
b
F
softer
harder
F=0
contact
z
c
sharp
dull
spherical probe
Elastic modulus (kPa)
T=25 v=6
37 2
37 2
25 6
37°C 10μm/s
d
T=25°C, v=6 μm/s
T=37°C, v=2 μm/s
F (nN)
Z (μm)
e
Lower force, T=37°C, v=2 μm/s
Higher force, T=25°C, v=6 μm/s
Sneddon model
Elastic modulus (kPa)
f
T=37°C, v=2 μm/s
F (nN)
Z (μm)
g
T=37°C, v=2 μm/s
Hertz model
Elastic modulus (kPa)
h
T=25°C, v =6μm/s
T=37°C, v =10μm/s
F (nN)
Z (μm)
i
T=37°C, v=10 μm/s
T=25°C, v=6 μm/s
Hertz model
Elastic modulus (kPa)

Figure 2

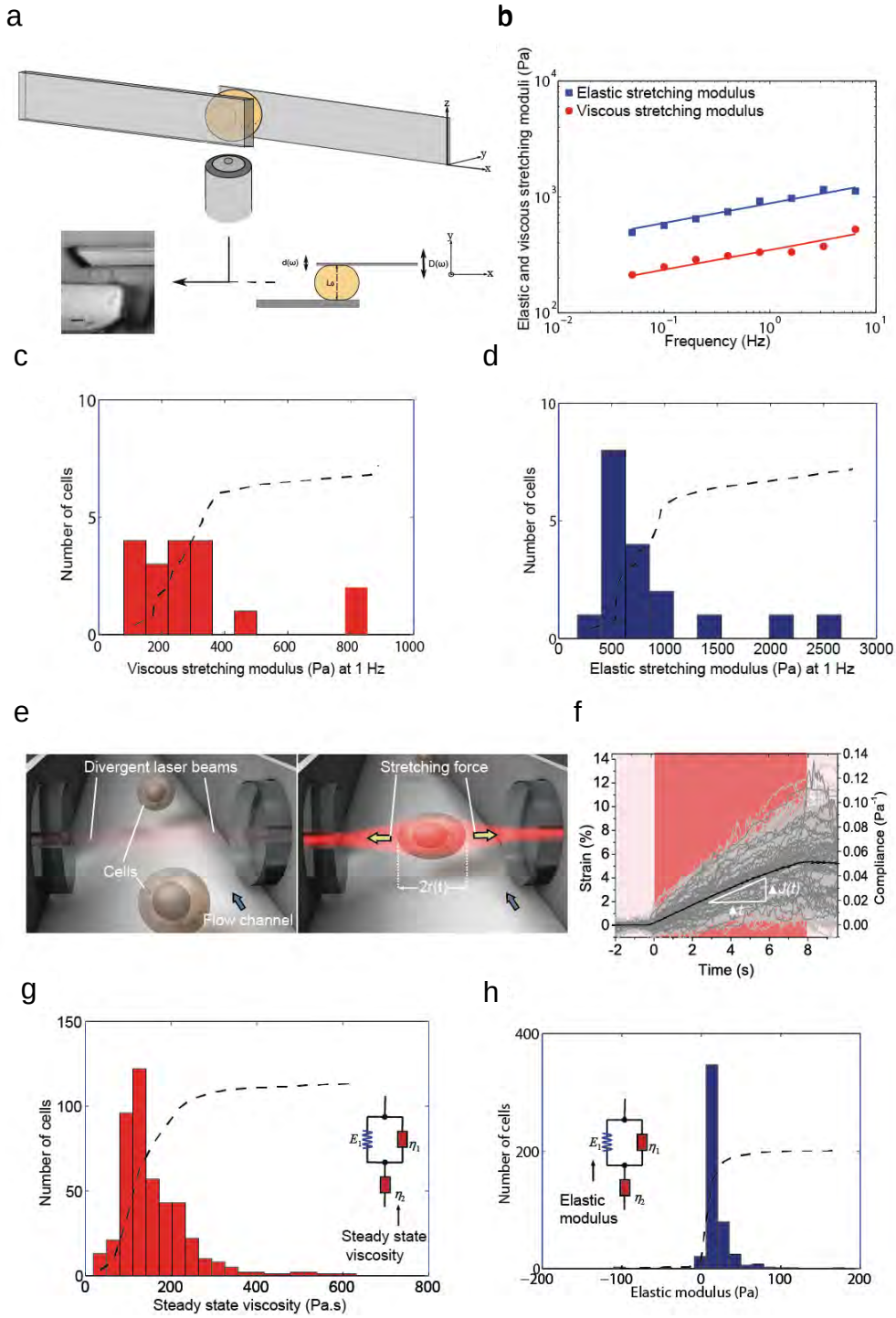
a
b
Elastic stretching modulus
Viscous stretching modulus
Elastic and viscous stretching moduli (Pa)
Frequency (Hz)
c
Number of cells
Viscous stretching modulus (Pa) at 1 Hz
d
Number of cells
Elastic stretching modulus (Pa) at 1 Hz
e
Divergent laser beams
Cells
Flow channel
Stretching force
2r(t)
f
Strain (%)
Compliance (Pa⁻¹)
Time (s)
g
Number of cells
Steady state viscosity
Steady state viscosity (Pa.s)
h
Number of cells
Elastic modulus
Elastic modulus (Pa)

Figure 3

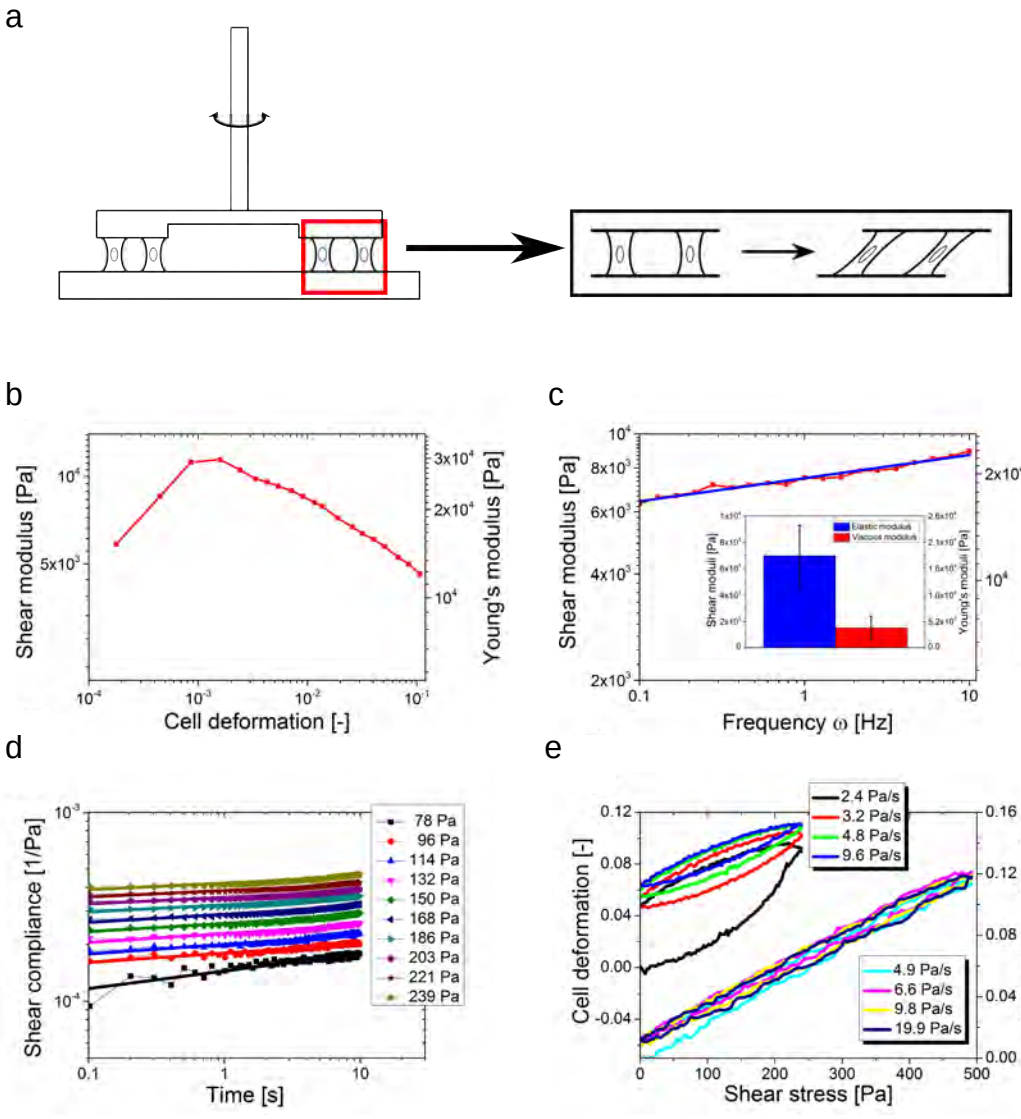
a
b
Shear modulus [Pa]
Young's modulus [Pa]
Cell deformation [-]
c
Shear modulus [Pa]
Young's modulus [Pa]
Frequency ω [Hz]
Elastic modulus
Viscous modulus
Shear moduli [Pa]
Young's moduli [Pa]
d
Shear compliance [1/Pa]
Time [s]
78 Pa
96 Pa
114 Pa
132 Pa
150 Pa
168 Pa
186 Pa
203 Pa
221 Pa
239 Pa
e
Cell deformation [-]
Shear stress [Pa]
2.4 Pa/s
3.2 Pa/s
4.8 Pa/s
9.6 Pa/s
4.9 Pa/s
6.6 Pa/s
9.8 Pa/s
19.9 Pa/s

Figure 4

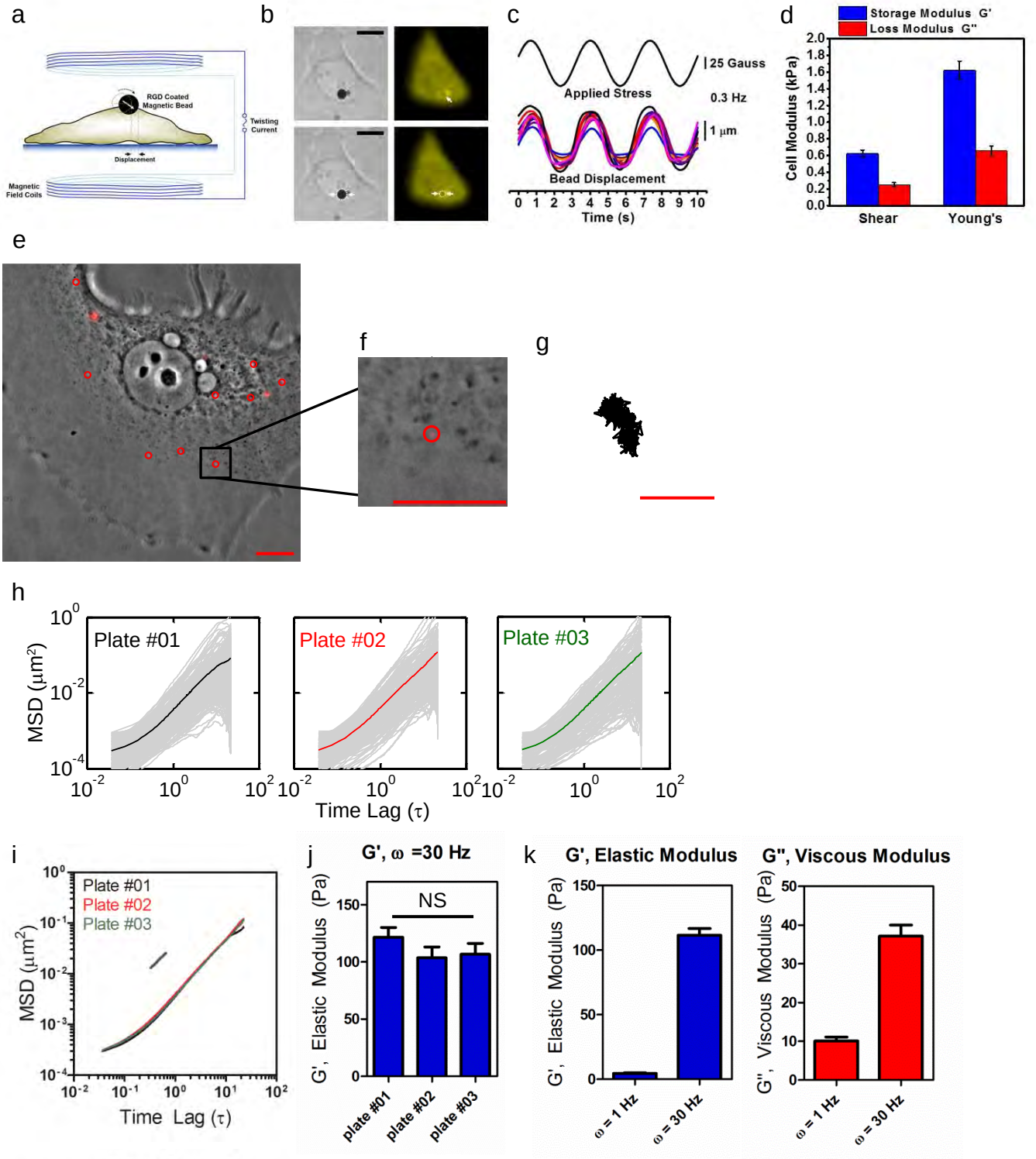
a
RGD Coated Magnetic Bead
Twisting Current
Displacement
Magnetic Field Coils
b
c
25 Gauss
Applied Stress
0.3 Hz
1 μm
Bead Displacement
Time (s)
d
Storage Modulus G'
Loss Modulus G"
Cell Modulus (kPa)
Shear
Young's
e
f
g
h
Plate #01
Plate #02
Plate #03
MSD (μm²)
Time Lag (τ)
i
Plate #01
Plate #02
Plate #03
MSD (μm²)
Time Lag (τ)
j
G', ω =30 Hz
NS
G', Elastic Modulus (Pa)
plate #01
plate #02
plate #03
k
G', Elastic Modulus
G", Viscous Modulus
G', Elastic Modulus (Pa)
G", Viscous Modulus (Pa)
ω = 1 Hz
ω = 30 Hz
l
Creep Compliance
Creep Compliance (1/Pa)
Time Lag (τ)
m
Numbers of particles
Accumulation of particles
MSD (μm²) @ 30Hz

Figure 5